

Bimodal distribution of mechanical properties on plasma sprayed nanostructured partially stabilized zirconia

R.S. Lima, A. Kucuk, C.C. Berndt *

Department of Materials Science and Engineering, State University of New York at Stony Brook, 306 Old Engineering Building, Stony Brook, NY 11794-2275, USA

Received 7 February 2001; received in revised form 18 May 2001

Abstract

The mechanical behavior of nanostructured partially stabilized zirconia (PSZ) coatings was evaluated via Knoop microhardness. The distribution of the microhardness values of the feedstock particles and coatings under a 10 g load were analyzed via Weibull statistics. The percentage of non-molten material was determined using scanning electron microscopy and image analysis. It was observed that the nanostructured coatings present a bimodal distribution in their Weibull plots, indicating the presence of two phases which are described as molten and non-molten. The presence of the bimodal distribution in the mechanical properties allows the prediction of microhardness values of these nanostructured coatings. © 2002 Elsevier Science B.V. All rights reserved.

Keywords: Thermal spray; Zirconia-yttria; Nanostructure; Thermal barrier coatings; Mechanical properties; Bimodal distribution

1. Introduction

Previous work [1] has demonstrated that it is necessary to maintain the nanostructured character of the nanostructured zirconia-yttria feedstock during the plasma spray process; i.e. the feedstock particles should not entirely melt during their passage through the spray jet. The mechanism of adhesion and cohesion of these nanostructured coatings was also observed and discussed in terms where the molten particles of the nanostructured feedstock act as a binder; i.e. enveloping and anchoring the non-molten particles in the coating microstructure [1].

Two forms of nanophase exist for the coatings examined in this work [1]; one evolving from the non-molten particles and the other resulting from the molten part of the nanostructured feedstock due to the rapid cooling rate and nucleation rates of molten thermal spray particles [2,3]. Analysis of the average grain size of thermal spray coatings via X-ray diffraction (XRD) can lead to difficulties in identifying: (i) the preserved

nanostructure of the feedstock; or (ii) the nanostructure created from the molten particles. Detailed information concerning both of these nanostructures can be achieved by examination of their fracture morphology via scanning electron microscopy (SEM). Regions resembling the molten feedstock will be similar to a traditional thermal spray structure [4–12]; whereas the regions resembling the nanostructured feedstock will be similar to the structure of the feedstock particles [1].

As a continuing study, the objective of this work is to investigate the mechanical properties of both molten and non-molten phases to establish the overall mechanical behavior of these coatings with respect to microhardness. The amount of non-molten phase in the coatings will also be investigated to correlate its relative proportion with the overall mechanical property behavior of the coatings.

2. Experimental procedure

The nanostructured PSZ ($ZrO_2-7wt.\%Y_2O_3$) experimental feedstock Nanox S4007 (Inframat, North Haven, CT) was plasma sprayed under different parameters in air on low carbon steel substrates with a

* Corresponding author. Tel.: +1-631-6328507; fax: +1-631-6328525.

E-mail address: cberndt@notes.cc.sunysb.edu (C.C. Berndt).

Metco 3MB (GH nozzle, powder port #2) plasma torch (Sulzer Metco, Westbury, NY). The spray parameters are listed in Table 1.

The Knoop microhardness measurements were performed under a 10 g load for 15 s (Tukon, Instron, Canton, MA) on the cross-section of the coatings and feedstock particles. The cross-sections of the samples were polished before the indentations. The coefficient of variation (CV) for these measurements on each sample stabilized at around 15–16 measurements and, therefore, 20 microhardness measurements were taken for each sample. This technique of sample size determination was also employed by Lin et al. [13,14].

The percentage of non-molten phase was determined via SEM on the cross-section of the coatings. A total of six SEM pictures were taken for each coating and an image analysis technique was used to determine the percentage of non-molten and molten material. The CV for these measurements stabilized after the analysis of four to five SEM pictures.

Table 1
The spraying parameters used for the Nanox S4007 feedstock (Metco 3MB)

Parameter	Set 1	Set 2	Set 3	Set 4
Power (kW)	42	42	42	42
Current (A)	600	600	600	500
Voltage (V)	70	70	70	70
Ar flow-plasma (slpm)	50	40	50	40
H ₂ flow-plasma (slpm)	11	12	11	12
Spray distance (cm)	8	8	10	10
Feed Rate (g min ⁻¹)	40	40	40	40
Ar flow-carrier gas (slpm)	3.5	3.5	3.5	3.5

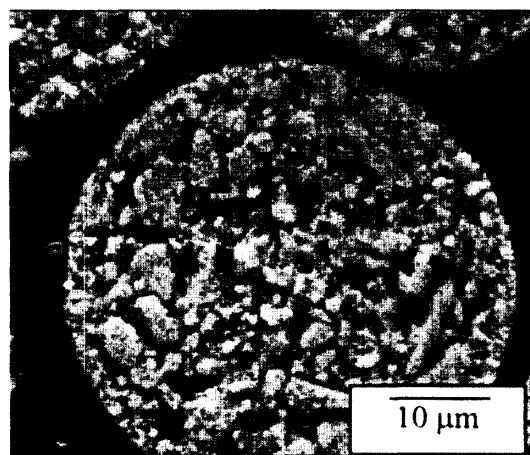


Fig. 1. Internal morphology (cross-section) of a typical nanostructured feedstock PSZ particle.

3. Results and discussion

3.1. Percentage of non-molten and molten feedstock

The cross-section of the nanostructured feedstocks was examined via SEM and makes it possible to distinguish regions where the non-molten material are present since there are similar morphological features between the feedstock and coating [1]. Fig. 1 shows the typical internal morphology of a nanostructured feedstock particle. Nanoceramic feedstocks typically contain agglomerates formed by clusters of nanograined particles [15]. It is important to notice the porosity formed by the cluster agglomeration associated with the nanostructured particle. This inherent particle porosity may produce important effects on coating microstructure, and mechanical [15] and thermo-mechanical properties.

No significant proportion of non-molten phase was found in the fracture surface of the Nanox 4007 coatings; whereas the Nanox S4007 coatings exhibited non-molten material in the coating microstructure [1]. The particle size distribution of the Nanox 4007 feedstock varies from 5 to 80 μm; whereas, the particle size distribution of the Nanox S4007 feedstock varies from 10 to 160 pm. Fig. 2 exhibits typical microstructures of the Nanox S4007 coatings. Each of the four micrographs represent the four sets of spray parameters applied to spray the feedstock [1]. On comparing the morphology of the feedstock particle (Fig. 1) with the coating morphology (Fig. 2), regions can be detected (as indicated on the micrographs) where non-molten feedstock particles are localized.

Feedstock which has been melted can be observed in regions where a large, dense and smooth structure is found. The non-molten feedstock is located in regions which have a similar morphology to that of the feedstock particle; i.e., an agglomeration of particles loosely bound to each other.

Using image analysis it was possible to separate and highlight the exact regions where the non-molten and molten particles were located. The percentage of non-molten and molten feedstock particles exhibited in the coatings for the spray parameters used are listed in Table 2. The percentage values correspond only to the 'solid part' of the coating; i.e. pores or voids were not taken into account.

The coating sprayed with the parameter set 3 revealed the highest amount of non-molten material; whereas the coating sprayed with parameter set 4 presented the lowest amount of non-molten phase.

Both molten and non-molten phases may present nanostructural characteristics. The nanostructure of the feedstock is formed by the agglomeration of individual nanoparticles within a colloidal suspension. It is assumed that a nanoparticle will consist of just one grain,

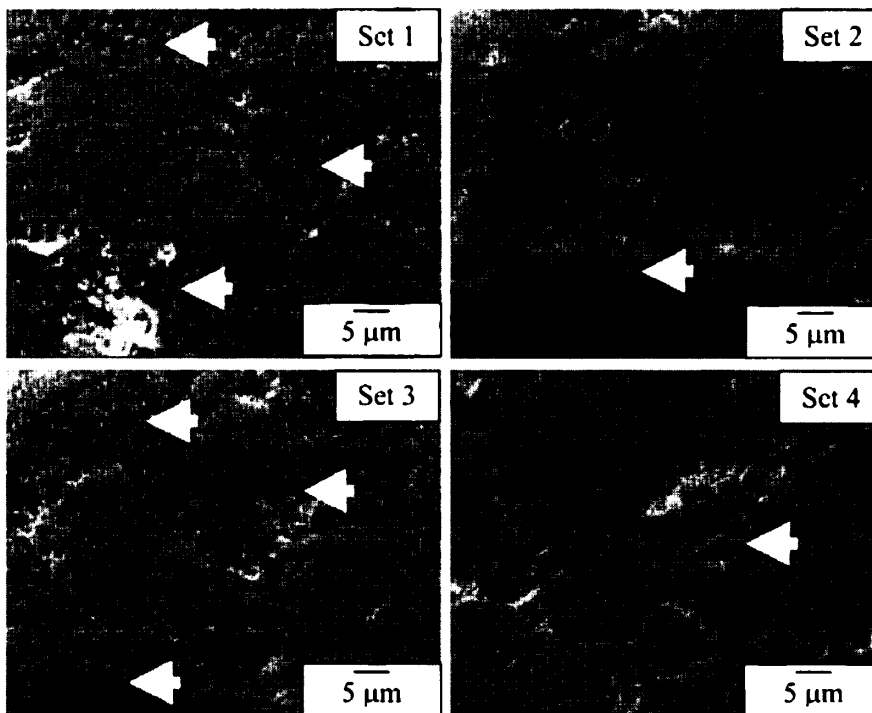


Fig. 2. Internal morphology (cross-section) of nanostructured PSZ coatings (spray parameters sets 1–4). The white arrows indicate the non-molten feedstock particles.

while a thermal spray splat is a microscopic entity which exhibits many nanosized grains highly bound among each other. This microstructural difference of nanograined agglomeration rather than a packed structure consisting of nanograins may produce a bimodal distribution in the mechanical properties of these coatings. This hypothesis is discussed in the following section.

3.2. Microhardness

The microhardness at a 10 g load for 15 s [16] for the nanostructured feedstock was 74 ± 16 HK. The measurements were taken on the cross-section of the polished nanostructured feedstock particles (Fig. 1). Observing Fig. 1, it is noticed that the typical feedstock particle exhibits a large pore volume. The agglomerated particles are loosely bound among each other and this is reflected in their low microhardness values. Due to the low average grain size of the feedstock particles (~ 100 nm) [1], it is expected that the feedstock hardness would exhibit high values. But according to Ref. [17], nanostructured agglomerated feedstock properties depend much more on the size and agglomeration conditions of the feedstock rather than its grain size. The present experimental results corroborate this prior work.

The microhardness values for the nanostructured coatings are shown in Fig. 3; as are those of a typical

Table 2

Percentage of non-molten and molten feedstock exhibit in the plasma-sprayed PSZ coatings for each spray parameter

Spray parameter	Non-molten feedstock (%)	Molten feedstock (%)
Coating-Set 1	46 ± 11	54 ± 12
Coating-Set 2	38 ± 14	62 ± 14
Coating-Set 3	52 ± 14	48 ± 13
Coating-Set 4	23 ± 14	77 ± 13

Note that non-molten and molten percentages add up to 100%. Note also that the percentage values correspond only to the 'solid part' of the coating; i.e. pores or voids were not taken into account.

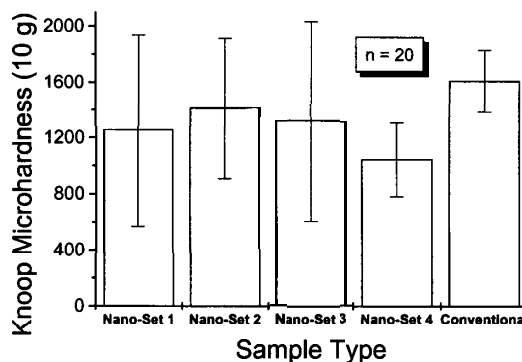


Fig. 3. Knoop microhardness values of the nanostructured and conventional coatings at 10 g load (cross-section).

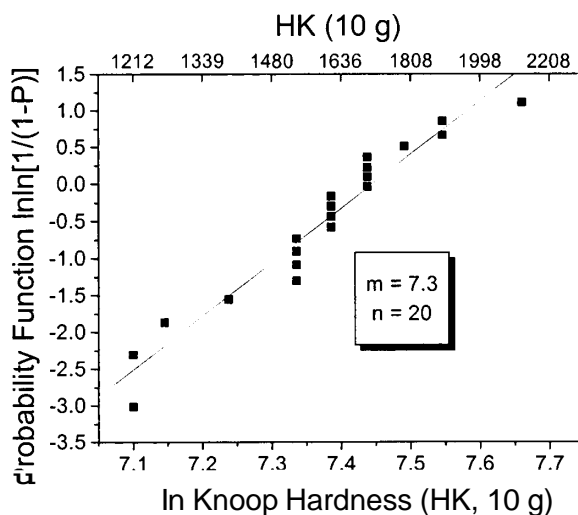


Fig. 4. Weibull plot of Knoop microhardness for the conventional coating.

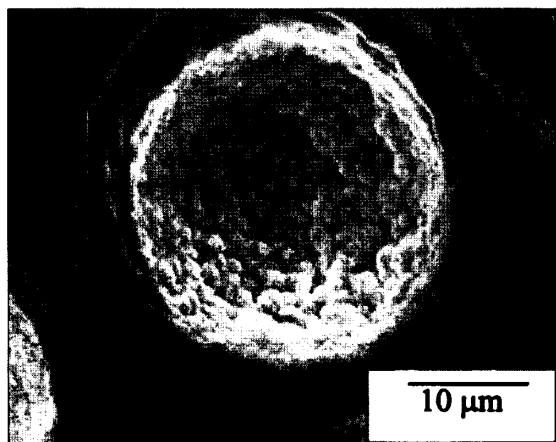


Fig. 5. Internal morphology (cross-section) of a conventional PSZ coating.

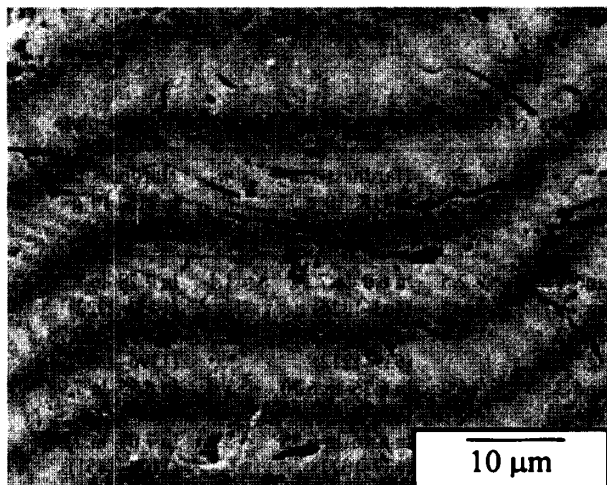


Fig. 6. Internal morphology (cross-section) of a conventional PSZ coating.

conventional PSZ coating (Metco 204NS). Due to the low load used (10 g), the indentation impression encloses a relatively small region of the coating. The major diagonal varied from 7 to 16 μm . These indentation sizes are on the order of a single or few splats of the coating. This minimizes the extent of defects, such as, coarse pores, splat boundaries, and microcracking enclosed within the indentation [18]. As a consequence, the intrinsic properties of the material are preferentially being measured. It should be cautioned that these intrinsic properties should not be considered as the bulk properties of a coating. However, as it will be pointed out in further sections, the intrinsic properties of distinct microstructural regions can be used to find the overall average properties of coatings.

All coatings have different microstructures and the sprayed feedstocks have distinctive features. Despite these different characteristics, when observing Fig. 3 it is noticed that the microhardness values are similar among the five different samples. As a consequence, the microhardness values preferentially represent, the physical characteristics of the material itself rather than the overall coating microstructure.

3.3. Bimodal distribution

As discussed previously, in the nanostructured coatings there are regions of molten and non-molten particles; which also may be considered as two phases. The hardness will be high in regions where there is a preferable concentration of molten particles; whereas, the hardness will be low in regions where there is a preferable concentration of non-molten particles. According to the SEM pictures, these regions of concentration are small and indentation sizes of several micrometers in length; e.g. 7–16 μm , would test these areas. Purely on the basis of probability, these two phases are measured during the 20 microhardness measurements and, therefore, the Weibull plots would be expected to show a bimodal distribution.

As a base of comparison, the Weibull plot of the conventional coating will be initially analyzed (Fig. 4). The feedstock Metco 204NS is termed as a hot-oven spherical particle (HOSP) and exhibits hollow sphere morphology (Fig. 5). According to Fig. 5, it is possible to observe that the typical particle is hollow, but its shell is dense. The mass of these particles is concentrated on the outer spherical surface and the process of particle melting is speculated by the authors to be more uniform in comparison to a non-hollow particle. Fig. 6 shows the typical microstructure of a conventional PSZ coating. It is possible to observe that the microstructure is dense and compact and quite different from the nanostructured coatings (Fig. 2). Indeed, on close examination of these very different microstructures (Fig. 6 compared to Fig. 2) it is difficult to understand why

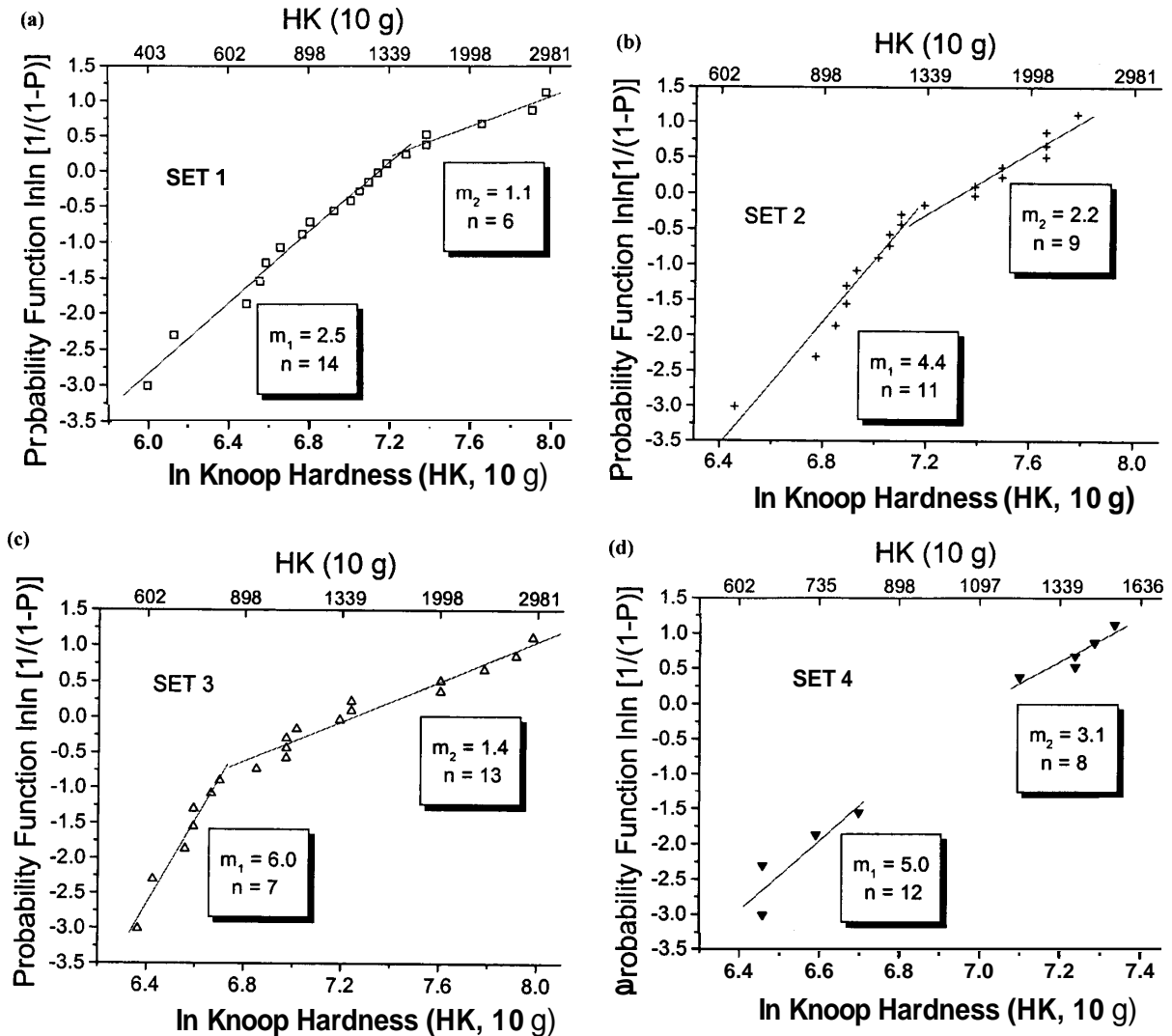


Fig. 7. (a) Weibull plot of Knoop microhardness for the nanostructured coating (Set 1). (b) Weibull plot of Knoop microhardness for the nanostructured coating (Set 2). (c) Weibull plot of Knoop microhardness for the nanostructured coating (Set 3). (d) Weibull plot of Knoop microhardness for the nanostructured coating (Set 4).

their hardness values (Fig. 3) are similar. However, it needs to be remembered that when using low loads, just a small volume of the material is analyzed. As a consequence, the intrinsic character of the zirconia-yttria is being assessed, rather than the extrinsic zirconia-yttria coating. If the indentation load is increased, then microstructural artifacts such as coarse porosity, cracks, and splat boundaries will play a more significant role in the materials property values. Consequently, they will have a higher weight on the hardness behavior [18] and significant different hardness values should be observed.

The Weibull plot of the Knoop hardness for the conventional coating (Fig. 4) does not exhibit a bimodal distribution. Instead, a single line with a Weibull modulus of 7.3 is noticed. The extreme values on the X-axis correspond to hardness values from 1212 to 2122 Knoop.

Table 3
Summary of results obtained from Weibull distribution plots

Set	m ,	Hardness range ln HK 10 g (HK 10 g)	m_2	Hardness range ln HK 10 g (HK 10 g)
Nano-1 (Fig. 7a)	2.5	ln 6.0–ln 7.19 (403–1326)	1.1	ln 7.28–ln 7.98 (1450–2922)
Nano-2 (Fig. 7b)	4.4	ln 6.46–ln 7.10 (639–1212)	2.2	ln 7.19–ln 7.78 (1396–2392)
Nano-3 (Fig. 7c)	6.0	ln 6.36–ln 6.70 (578–812)	1.4	ln 6.85–ln 7.98 (943–2922)
Nano-4 (Fig. 7d)	5.0	ln 6.46–ln 6.93 (639–1022)	3.1	ln 7.01–ln 7.34 (1108–1451)
Conventional (Fig. 4)	NA	NA	7.3	ln 7.10–ln 7.66 (1212–2122)

Table 4
Microhardness values from the non-molten and molten regions of the nanostructured coating microstructure

Microstructural region	Microhardness value (HK 10 g)
Non-molten	893 ± 222
Molten	1699 ± 563

The Weibull plots for the Knoop hardness for the nanostructured coatings are shown in Fig. 7 and indicate that nanostructured coatings exhibit a bimodal distribution of hardness. Table 3 summarizes the information provided by these figures.

In order to determine the exact point where the slopes m_1 and m_2 are localized in Fig. 7, the R^2 statistics was determined with respect to the number of measurements. R^2 was plotted for 3, 4, 5, etc. measurements of $\ln[1/(1 - P)]$ until all the 20 measurements were taken into account. For each sample, two curves were plotted. One starting from the ascending values, and the second curve for descending values. For each sample, there will be a point where the R^2 maximum of the two graphs intercept each other. This data value corresponds to a transition point where one data set is statistically more valid than neighboring data sets.

When comparing Fig. 4 with Fig. 7 and the results of Table 3, it is noticed that the conventional coating (Fig. 4) has a range of microhardness values from 1212 to 2122 HK. However, the nanostructured coatings (Fig. 7) show values similar to this range in the low slope regions of the Weibull plots. Since the conventional coating primarily represents the behavior of fully molten particles, this observation indicates that the low slope regions of the Weibull plots reflect microstructural features of the nanostructured feedstock which are molten. On the other hand, the high slope regions at low hardness values represent the non-molten feedstock particles in the coating microstructure.

It can be pointed out that Lin et al. [13,14] also analyzed the microhardness behavior of plasma sprayed conventional zirconia coatings via Weibull distribution plots and Weibull modulus. No noticeable bimodal distribution was noticed in this prior work.

Table 5
Microhardness prediction by employing Eq. (1) (all values in HK 10 g)

Set	H_1	f_{H_1}	H_2	f_{H_2}	Result	Predicted microhardness
1	893 + 222	0.46	1699 + 563	0.54	1734	1328 ± 574
	893 - 222	0.46	1699 - 563	0.54	922	
2	893 + 222	0.38	1699 + 563	0.62	1826	1393 ± 613
	893 - 222	0.38	1699 - 563	0.62	959	
3	893 + 222	0.52	1699 + 563	0.48	1666	1280 ± 545
	893 - 222	0.52	1699 - 563	0.48	894	
4	893 + 222	0.23	1699 + 563	0.77	1998	1514 ± 685
	893 - 222	0.23	1699 - 563	0.77	1029	

Since the non-molten particles exhibit low hardness, the nanostructured material may lead to the improvement of compliance in TBCs properties, such as; residual stress and thermal shock.

3.4. Prediction of mechanical properties

Based on the fact that the two-slope region represents the presence of non-molten and molten particles, the following hypothesis is proposed. These coatings can be considered as a composite consisting of two materials: molten and non-molten particles. Mechanical properties, such as microhardness, could be predicted on knowledge concerning the microhardness and quantity of each individual phase. The final coating microhardness value would be predicted according to a 'rule of mixtures' approach; i.e.

$$\text{Predicted microhardness} = H_1 \cdot f_{H_1} + H_2 \cdot f_{H_2} \quad (1)$$

In Eq. (1), H_1 and H_2 are the microhardness values of the non-molten and molten regions; and f_{H_1} and f_{H_2} are the percentages (fractions) of the non-molten and molten regions in the overall coating microstructure; respectively.

The percentage of non-molten and molten regions was determined via SEM assisted by image analysis and the results are listed in Table 2. All microhardness measurements enclosed in the high (m_1) and low (m_2) slope regions were averaged to determine the microhardness values of the two different regions. A total of 44 and 36 microhardness values for the non-molten and molten regions were taken for average determination; respectively. The results are summarized in Table 4. The microhardness for the non-molten particles embedded in the coating microstructure is higher than that for the feedstock. This probably occurs due to effects of particle densification during plasma spraying and compaction upon impact against the substrate. The predicted microhardness values determined via Eq. (1) are listed in Table 5.

Fig. 8 shows a comparison between the experimental and predicted microhardness for the nanostructured PSZ coatings. It is important to point out that the

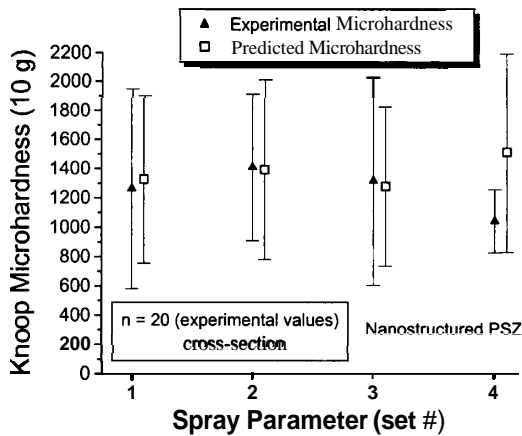


Fig. 8. Comparison between experimental and predicted microhardness values for the nanostructured PSZ coatings.

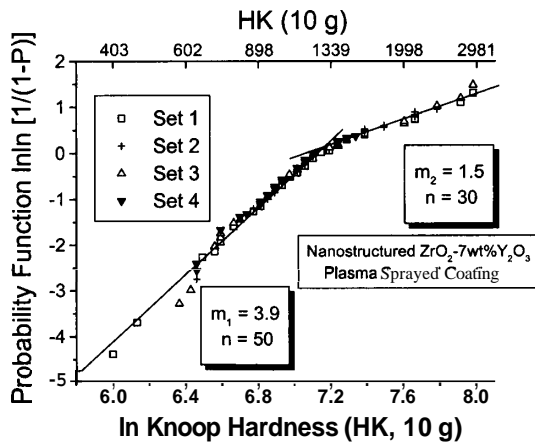


Fig. 9. Weibull plot of Knoop microhardness for all nanostructured coatings (Sets 1–4).

model applied does not account for coarse porosity effects. As discussed in Section 3.2; indentation sizes on the order several micrometers minimizes these microstructural features [18]. But if indentation loads higher than 10 g are employed, the indentation impression sizes will become larger. Therefore, coarse porosity effects will show some influence and they have to be a part of the model. In Fig. 8 it is possible to observe good agreement between the experimental and predicted values. The 'goodness-of-fit' test was employed to compare the predicted and experimental values. Since the P-value (0.699) is greater than the value of level of significance (0.05), there is not a statistically significant difference between the two distributions at the 95% confidence level; which supports the approach employed in this work.

The microhardness values of the coatings do not exhibit significant differences (Fig. 8). However, the Weibull moduli for each coating and region present significant variations (Table 2, Fig. 7) due to the pres-

ence of the two phases (Table 2). These characteristics will affect the overall mechanical properties in distinctive ways. Therefore, measurements of average microhardness and S.D., per se, are poor indicators for understanding the mechanical behavior associated with hardness. A more thorough microstructural and statistical investigation, such as Weibull analysis, is necessary.

It is interesting to notice the bimodal behavior of samples 3 and 4 since these have the highest and lowest proportions of non-molten particles in the coating microstructure; respectively (Table 2). Sample 3 (Fig. 7c) has a very distinctive bimodal distribution, whereas sample 4 (Fig. 7d) barely shows this characteristic; being similar to the behavior of the conventional sample (Fig. 4). Thus, when the proportion of non-molten particles in the coating microstructure decreases, i.e. the coating consists mainly of molten particles, then the nanostructured coating tends to display behavior similar to the conventional coating, and the bimodal distribution disappears.

Other mechanical properties, such as, elastic modulus and fracture toughness [18–21] can also be measured via indentation techniques. Therefore, it is likely that the elastic modulus and fracture toughness of these coatings, can be predicted by employing the same model and method described in this work.

Another analysis treated all the data sets of the nanostructured coatings as belonging to the same global population. Therefore, these four data sets were pooled, Fig. 9. A bimodal distribution is evident and it is possible to observe the data points from all the four spray parameters distributed along the plot. The bimodal distribution of mechanical properties is inherent to the nanostructured coatings; if at least some part of the nanostructured feedstock is kept intact after the plasma spraying process.

The values of m , and m_2 are 3.9 and 1.5, respectively. The averages of m , and m_2 taken from Fig. 7 are 4.5 and 1.9, respectively, and indicate a close correspondence that corroborates the bimodal nature of this class, of materials.

3.5. Future possibilities

The distinct bimodal character of the nanostructured PSZ coatings presents an opportunity for TBC microstructural control in a materials engineering endeavor to control their failure mechanisms. Thermal spray ceramic coatings start sintering at high temperatures (≈ 1000 °C). McPherson [2,3,22,23] has discussed the effects of sintering on the mechanical properties and thermal conductivity of thermal spray coatings. There are two morphologies for the porosity present in a coating. First, there is the coarse porosity (3 to 10 μm) associated with filling defects in the coating structure, which is generally cause by semi-molten particles. Sec-

only, there are fine planar pores (0.01–0.1 μm) located in between splats arising from gas entrapped beneath liquid droplets during coating formation.

Thermal spray coatings have lower values of mechanical properties and thermal conductivity when compared to bulk samples for the same levels of coarse porosity. These lower values can be explained in terms of a model for the coating microstructure involving limited regions of 'good' contact between splats. At high temperatures, changes in coarse porosity may be negligible but healing of the fine planar pores occurs [2,3,22,23]. When this does happen, the degree of contact between splats increases and thereby causes: (i) a higher elastic modulus and hardness in the coating structure; and (ii) an increase in thermal conductivity [2,3,22–24]23. These changes in material characteristics are detrimental to the coating integrity during service.

Some researchers [25–27] have been working on this issue for TBCs. A clear relationship between coating design and life prediction with these temperature dependent properties was established by studying the variation in coating elastic modulus, hardness, and thermal conductivity due to sintering effects.

With special reference to the present work, nanostructured coatings may reduce temperature dependent effects on elastic modulus, hardness, and thermal conductivity. Observing Figs. 1 and 2, it is noticed that the nanostructured feedstock particle is porous, and this intrinsic porosity will be retained in the coating microstructure within the non-molten particles. Weertman et al. [15] discuss the effects of this intrinsic porosity in agglomerated nanostructured feedstocks on sintering. Since the nanostructured feedstock particles have bonded clusters of nanograins (Fig. 1), sufficient pressure must be exerted to allow particle and cluster rearrangement in order to attain high densities. Consequently, it appears that the morphology of nanostructured agglomerated particles offer an activation barrier to impede sintering. This phenomenon was also observed by Yan and Rhodes [17].

Thus, the presence of non-molten, nanostructured feedstock particles in the coating microstructure may create a barrier against sintering effects on elastic modulus, hardness, and thermal conductivity. As consequence, it is thought that the bimodal distribution may be retained at high temperatures, thereby enhancing coating integrity due to compliance effects. The particle morphology might also help to avoid grain growth at high temperatures. Another important characteristics of nanostructured materials concern their superplasticity [15] and this property, if present in these coatings, may be beneficial with respect to improving the coating compliance under the operational heat flux environment.

4. Conclusions

The experimental observations of this work are listed below:

(1) The microhardness of the nanostructured PSZ feedstock is low due to the weak agglomeration and relatively high porosity of the nanostructured agglomerates.

(2) The nanostructured PSZ coatings demonstrate a bimodal distribution, as evidenced by their Weibull plots, with respect to the mechanical properties. A high slope (high Weibull modulus and low hardness values) represents non-molten/semi-molten feedstock particles. A low slope (low Weibull modulus and high hardness values) represents fully molten particles.

(3) The conventional PSZ coating does not present a bimodal distribution in the Weibull plot with respect to the mechanical properties. A mono-modal distribution is observed.

(4) The microhardness of the nanostructured PSZ coatings can be predicted by a rule of mixtures law, in which a coating is considered as a two-phase composite.

(5) Microhardness measurements per se are not sufficient to characterize the mechanical properties of nanostructured coatings. A statistical analysis such as Weibull distribution is necessary for a more complete understanding of the influence of the microstructure on the mechanical properties.

(6) When the percentage of non-molten nanostructured feedstock particles in the coating microstructure decreases, the bimodal distribution tends to disappear, and the nanostructured coating tends to behave as a conventional one.

Acknowledgements

This work was supported from a subcontract from the University of Connecticut under Office of Naval Research contract number N00014-98-C0100.

References

- [1] R.S. Lima, A. Kucuk, C.C. Berndt, Mater. Sci. Eng. A313 (2001) 75–82.
- [2] R. McPherson, Surf. Coat. Technol. 39/40 (1989) 173.
- [3] R. McPherson, Thin Solid Films 83 (1981) 297.
- [4] L. Pawlowski, The Science and Engineering of Thermal Spray Coatings, Wiley, West Sussex, UK, 1995.
- [5] V. Wilms, H. Herman, Thin Solid Films 39 (1976) 251.
- [6] S. Safai, H. Herman, Thin Solid Films 45 (1977) 295.
- [7] D. Harmsworth, R. Stevens, J. Mater. Sci. 27 (1992) 616.
- [8] R.B. Heimann, J. Thermal Spray Technol. 8 (4) (1999) 597.
- [9] A. Geibel, L. Froyen, L. Delaey, K.U. Leuven, J. Thermal Spray Technol. 5 (4) (1996) 419.

- [10] R. Hamacha, P. Fauchais, F. Nardou, J. Thermal Spray Technol. 5 (4) (1996) 431.
- [11] A. Haddadi, F. Nardou, P. Fauchais, A. Grimaud, A.C. Leger, in: C.C. Berndt (Ed.), *A United Forum for Scientific and Technological Advances*, ASM International, Materials Park, OH, USA, 1997, p. 671.
- [12] A. Haddadi, F. Nardou, A. Grimaud, P. Fauchais, in: C.C. Berndt, S. Sampath (Eds.), *Thermal Spray Science and Technology*, ASM International, Materials Park, OH, USA, 1995, p. 249.
- [13] C.K. Lin, C.C. Berndt, J. Mater. Sci. 30 (1995) 111.
- [14] C.K. Lin, C.C. Lin, C.C. Berndt, J. Am. Ceram. Soc. 78 (5) (1995) 1406.
- [15] J.R. Weertman, D. Farkas, K. Hemker, H. Kung, M. Mayo, R. Mitra, H. Van Swygenhoven, MRS Bull., February (1999) 44.
- [16] Standard Test Method for Microhardness of Materials, ASTM E 384-89.
- [17] M.F. Yan, W.W. Rhodes, Mater. Sci. Eng. 61 (1983) 59–66.
- [18] J.P. Singh, M. Sutaria, M. Ferber, Ceram. Eng. Sci. Proc. 18 (4b) (1997) 191.
- [19] D.B. Marshall, T. Noma, A.G. Evans, Commun. Am. Ceram. Soc. (1982), C-175–C-176.
- [20] G.R. Anstis, P. Chantikul, B.R. Lawn, D.B. Marshall, J. Am. Ceram. Soc. 64 (9) (1981) 533.
- [21] P. Chantikul, G.R. Anstis, B.R. Lawn, D.B. Marshall, J. Am. Ceram. Soc. 64 (9) (1981) 539.
- [22] R. McPherson, Thin Solid Films 112 (1984) 89.
- [23] R. McPherson, Thin Solid Films 97 (1982) 201.
- [24] P. Boch, D. Fargeot, C. Gault, F. Platon, Rev. Int. Hautes Temper. Refract. 18 (1981) 85.
- [25] D. Zhu, R.A. Miller, MRS Bull., July (2000) 43.
- [26] D. Zhu, R.A. Miller, J. Thermal Spray Technol. 9 (2) (2000) 175.
- [27] D. Zhu, R.A. Miller, Surf. Coat. Technol. 108–109 (1998) 114.